Research Square

Preprints are preliminary reports that have not undergone peer review.
They should not be considered conclusive, used to inform clinical practice,
or referenced by the media as validated information.

Concurrent inhibition of JAK2 and FLT3 by pacritinib is a promising therapeutic strategy for hepatocellular carcinoma

Jisoo Kim
Korea Research Institute of Chemical Technology
Yonghyo Kim
Korea Research Institute of Chemical Technology
Hyeran Shin
Korea Research Institute of Chemical Technology
Hyun-Woo Jeong
Max Planck Institute for Molecular Biomedicine
Yong-Hee Cho
y-hcho@krict.re.kr

Korea Research Institute of Chemical Technology

Research Article

Keywords: HCC, JAK2, FLT3, Anticancer, Tumor organoid

Posted Date: October 31st, 2026

DOI: https://doi.org/10.21203/rs.3.rs-11231431/v1

License: This work is licensed under a Creative Commons Attribution 4.0 International License.
Read Full License

Additional Declarations: No competing interests reported.

Abstract

Background

Hepatocellular carcinoma (HCC) remains a major therapeutic challenge due to the limited efficacy of current systemic therapies with substantial intra-tumoral heterogeneity. The modest clinical benefit of multi-kinase inhibitors such as sorafenib underscores the need for alternative multi-kinase therapeutic strategies. Here, we investigated the therapeutic potential of concurrent JAK2 and FLT3 inhibition by pacritinib in HCC.

Methods

The antitumor effects of pacritinib were evaluated in HCC cell lines, HCC organoids, and an organoid-derived xenograft model, with sorafenib used as a comparator. Single-cell RNA sequencing was performed in a representative HCC organoid to characterize treatment responses across transcriptionally distinct tumor cell populations.

Results

Concurrent inhibition of JAK2 and FLT3 by pacritinib potently suppressed HCC cell growth, accompanied by inhibition of JAK2/STAT3 and FLT3 signaling, and showed greater antitumor activity than sorafenib in both HCC cell lines and organoids. Marked tumor growth inhibition was also observed in an organoid-derived xenograft model. Single-cell RNA sequencing of a representative HCC organoid revealed consistent responses across three transcriptionally distinct tumor cell populations, with suppression of cell-cycle progression and DNA replication programs.

Conclusions

These findings support the therapeutic potential of pacritinib in HCC and suggest that concurrent inhibition of JAK2 and FLT3 may represent a promising strategy for molecularly heterogeneous HCC.

Introduction

Hepatocellular carcinoma (HCC) is the sixth most commonly diagnosed malignancy and the third leading cause of cancer-related mortality worldwide (1, 2). Despite substantial advances in systemic therapies over the past decade, the prognosis of patients with advanced HCC remains poor, with a 5-year survival rate below 20% (3). Immune checkpoint inhibitor (ICI)-based combination therapies, particularly atezolizumab plus bevacizumab, have become the standard first-line treatment for advanced HCC (4, 5). However, their clinical benefit remains limited, achieving an objective response rate of only approximately 27%, while most patients eventually develop primary or acquired resistance (3, 4, 6). For

patients who fail to benefit from immunotherapy, multi-kinase inhibitors, including sorafenib and lenvatinib, remain the principal treatment option (7). Nevertheless, these agents provide only modest survival benefits, underscoring an urgent need to identify more effective therapeutic targets and develop improved targeted therapies for advanced HCC.

Sorafenib and lenvatinib, the two principal multi-kinase inhibitors approved for advanced HCC (8, 9), simultaneously inhibit multiple receptor tyrosine kinases involved in tumor proliferation, angiogenesis, and survival, including VEGFRs, PDGFRs, FGFRs, KIT, RET, FLT3, and RAF kinases (10). Despite their broad kinase inhibition profiles, the clinical benefits of these agents remain modest (11, 12). Sorafenib achieves an objective response rate of approximately 10% and prolongs median overall survival by only 2–3 months compared with placebo (13), whereas lenvatinib improves the objective response rate to approximately 20–25% but provides overall survival comparable to sorafenib (12). Consequently, durable clinical responses are limited to a subset of patients, with disease progression eventually occurring in the majority of cases. These clinical outcomes suggest that broad inhibition of multiple kinases does not necessarily translate into sustained therapeutic efficacy and underscore the importance of defining the specific kinase targets that contribute most substantially to antitumor activity in HCC. A better understanding of such therapeutically relevant kinase targets may enable more rational selection and combination of kinase-directed therapies and ultimately improve the clinical efficacy of targeted treatment for HCC.

The FMS-like tyrosine kinase 3 (FLT3) is a receptor tyrosine kinase that regulates cellular proliferation, survival, and differentiation through downstream signaling pathways, including STAT, PI3K/AKT, and MAPK (14). Aberrant activation of FLT3 signaling promotes malignant cell proliferation and survival and is a well-established oncogenic driver and therapeutic target, particularly in acute myeloid leukemia (AML) (15). In HCC, FLT3 expression varies considerably across HCC tumors, with copy-number loss and reduced FLT3 expression frequently observed (16). FLT3 is also recognized as one of the kinase targets of sorafenib (10). Notably, Low FLT3 expression has been associated with limited clinical benefit from sorafenib (16), suggesting that FLT3 expression may influence therapeutic responses to sorafenib in HCC. These findings highlight the need for alternative therapeutic strategies for patients with FLT3-low HCC who derive limited benefit from sorafenib.

The Janus kinase 2 (JAK2) signaling pathway is a key oncogenic pathway involved in the development and progression of multiple cancers (17). Aberrant activation of JAK2 can activate multiple downstream signaling pathways, including STAT3 and PI3K/AKT, thereby promoting tumor cell proliferation, survival, stemness, angiogenesis, metastasis, immune evasion, and resistance to anticancer therapies (18, 19). In HCC, dysregulated JAK2 signaling and its downstream STAT3 and PI3K/AKT pathways have been implicated in tumor initiation and progression and are closely associated with therapeutic resistance (20, 21). Despite evidence supporting JAK2 as a therapeutic target in HCC, no JAK2-targeted therapy has been approved for the treatment of HCC.

In this study, given the therapeutic relevance of JAK2 and FLT3 in HCC and their potential association with the therapeutic response to sorafenib, we investigated pacritinib, a clinically available JAK2 and FLT3 inhibitor (22, 23), as an alternative treatment strategy for HCC. We evaluated the antitumor activity of pacritinib across multiple HCC cell lines and three-dimensional HCC organoid models representing tumoral heterogeneity (24, 25), followed by in vivo validation using an HCC organoid-derived xenograft model. Single-cell RNA sequencing of a representative HCC organoid model further revealed comparable responses to pacritinib across molecularly distinct tumor cell populations, characterized by consistent suppression of cell-cycle progression and DNA replication, with no prominent population exhibiting an intrinsically resistant phenotype. Notably, pacritinib exhibited greater antitumor activity than sorafenib across HCC models, supporting its potential as an alternative therapeutic option to sorafenib. Together, these findings provide preclinical evidence supporting pacritinib as a promising therapeutic strategy for molecularly heterogeneous HCC, particularly as a potential alternative to sorafenib.

Methods

Cell cultures

Human HCC cell lines (HepG2, Hep3B, Huh7, PLC/PRF5, SNU-886, SNU-878, SNU-761, SNU-739, SNU-3160(150315)) and human HCC primary cells (SNU-398, SNU-449, SNU-423, SNU-182, SNU-475, SNU-354, SNU-368, SNU-387) were purchased from the Korean Cell Line Bank (Seoul, Republic of Korea) and were cultured in RPMI1640 (Hyclone, UT, USA) or DMEM (Hyclone) supplemented with 10% fetal bovine serum (Gibco, CA, USA) and 1% penicillin/streptomycin at 37°C in 5% CO2.

Western blotting

Western blotting
Cells were washed with ice-cold PBS and lysed in radioimmunoprecipitation assay (RIPA) buffer supplemented with protease and phosphatase inhibitor cocktail. Cell lysates were incubated on ice, clarified by centrifugation, and mixed with 5× SDS sample buffer followed by heat denaturation. Proteins were separated by 8–10% sodium dodecyl sulfate-polyacrylamide gel electrophoresis (SDS-PAGE) and transferred onto nitrocellulose membranes (Bio-Rad, CA, USA).

After blocking with either 10% skim milk or 5% bovine serum albumin in Tris-buffered saline containing 0.1% Tween-20 (TBST), membranes were incubated with primary antibodies: anti-JAK2 (Cell Signaling Technology, MA, USA, #3230), anti-phospho-JAK2 (Tyr221; Cell Signaling Technology, #3774), anti-FLT3 (Thermo Fisher Scientific, MA, USA, #PA5-34448), anti-phospho-FLT3 (Tyr591; Cell Signaling Technology, #3461), anti-STAT3 (Cell Signaling Technology, #9139), anti-phospho-STAT3 (Tyr705; Cell Signaling Technology, #9145), anti-AKT (Cell Signaling Technology, #9272), anti-phospho-AKT (Ser473; Cell Signaling Technology, #9271), anti-cleaved caspase 3 (Cell Signaling Technology, #9664), anti-cleaved PARP1 (Abcam, Cambridge, UK, #ab32064), and anti-β-actin (Thermo Fisher Scientific, #PA1-183),

followed by the appropriate horseradish peroxidase-conjugated secondary antibodies. Protein bands were detected using SuperSignal™ West Femto Maximum Sensitivity Substrate (Thermo Fisher Scientific, #34095). Chemiluminescent signals were acquired using the iBright imaging system (Thermo Fisher Scientific) and quantified with iBright Analysis software (Thermo Fisher Scientific).

Cell proliferation and viability assay

Cells were seeded into 96-well plates for cell proliferation or viability assays. For proliferation assays, cells were plated into separate plates for each time point (0, 24, 48, and 72 h). For viability assays, cells were allowed to attach overnight and then treated with the indicated concentrations of pacritinib and sorafenib for 72 h. Cell proliferation and viability were assessed using the CytoX Cell Viability Assay Kit (LPS Solution, Daejeon, Korea, #CYT3000) according to the manufacturer's instructions

Colony formation assay

Cells were seeded into 12-well plates and allowed to attach overnight before treatment with pacritinib or sorafenib. The culture medium was replaced every 3 days, and cells were cultured until visible colonies had formed. Colonies were fixed with 3.7% formaldehyde and stained with 0.5% crystal violet. Colony formation was quantified by measuring both the number and area of colonies using ImageJ software (National Institutes of Health, MD, USA).

Lentiviral transduction and shRNA knockdown

Lentiviral particles were produced in Lenti-X 293T cells by calcium phosphate-mediated transfection using 16 μg of shRNA-expressing pLKO.1-EGFP-puro transfer vector, 5 μg of psPAX2 packaging plasmid, and 5 μg of pMD2.G envelope plasmid. The plasmid mixture was combined with 2 M $CaCl_2$ and 2× HEPES-buffered saline and added dropwise to Lenti-X 293T cells cultured in serum-free DMEM. After incubation for 8 h at 37°C, fetal bovine serum was added to the culture medium, and the medium was replaced with fresh complete DMEM on the following day. Viral supernatants were harvested at 48 and 72h after transfection, combined, and passed through a 0.45-μm filter. Target cells were transduced with the filtered viral supernatant in the presence of 8 μg/mL polybrene and centrifuged at 1,000 × g for 90 min, and subsequently selected with puromycin. The target sequences of the shRNAs were as follows: nontargeting control (NTC), 5'-CCTAAGGTTAAGTCGCCCTCGCTC-3'; shJAK2 #1, 5'-GCAGAATTAGCAAACCTTATACTC-3'; shJAK2 #2, 5'-CTGGTATGCTCCAGAATCACTGACAGAGA-3'; shFLT3 #1, 5'-GGTGTCGAGCAGTACTCTAAA-3'; and shFLT3 #2, 5'-GCATCCCAGTCAATCAGCTTT-3'. All shRNAs were cloned into the pLKO.1-EGFP-puro vector using AgeI and EcoRI restriction sites.

Apoptosis analysis by flow cytometry

Cells were seeded and allowed to attach overnight before treatment with pacritinib. After treatment, both floating and adherent cells were collected, washed with Annexin V binding buffer (10 mM HEPES, 140 mM NaCl, and 2.5 mM $CaCl_2$; pH 7.4), and stained with FITC Annexin V (BD Biosciences, CA, USA, #556420) and propidium iodide (PI; BD Biosciences, #556463) according to the manufacturer's instructions. After incubation for 15 min at room temperature in the dark, samples were analyzed within 1 h using a BD FACSCanto™ II flow cytometer (BD Biosciences). Data were analyzed using BD FACSDiva Software version 8.0 (BD Biosciences).

Single cell RNA Sequencing Analysis

Control and pacritinib-treated HCC organoid #6 were dissociated into single cells, labeled with BD Hu Single Cell Sample Multiplexing Kit (BD Biosciences #633781) and loaded onto a microwell cartridge of the BD Rhapsody Express system (BD) according to the manufacturer’s instructions. Single cell and mRNA captures were performed using the BD Rhapsody Cartridge kit (BD Biosciences #633733), Cartridge Enhanced Reagent kit (BD Biosciences #664887), and BD Rhapsody cDNA kit (BD Biosciences #633773). Whole-transcriptome libraries were subsequently generated using the BD Rhapsody WTA Reagent Kit (BD Biosciences #633802) following the manufacturer’s instructions.

The final indexed libraries were sequenced on an Illumina NextSeq 2000 platform using the P2 Reagent Kit (Illumina, #20100987, 100 cycles) with 50 bp + 75 bp paired-end reads and an 8-bp single index, targeting a sequencing depth of more than 20,000 reads per cell for each sample.

The FASTQ-format sequencing raw data was initially processed using the BD Rhapsody Sequencing Analysis Pipeline (VELSERA, version 1.2). Reads were aligned to the hg38 human reference genome using the BD Rhapsody reference package (RhapRef_Human_WTA_2025-10). Data normalization, dimensionality reduction and visualization were performed in R using the Seurat package (version 4.4.0), unless otherwise specified.

Cells corresponding to SampleTag07_hs and SampleTag08_hs were assigned to the control and pacritinib-treated groups, respectively. Mitochondrial transcript content was calculated using genes beginning with MT-, and cells were retained when they contained fewer than 7,000 detected genes and less than 40% mitochondrial reads. After quality control, 8,070 cells were included in the analysis, consisting of 4,267 control cells and 3,803 pacritinib-treated cells.

Gene expression counts were log-normalized with a scale factor of 10,000. For each sample, 2,000 highly variable genes were identified using the variance-stabilizing transformation method. KEGG cell-cycle genes were removed from the variable feature set before integration to reduce cell-cycle-driven clustering. Control and pacritinib-treated cells were integrated using Seurat anchor-based integration using FindIntegrationAnchors and IntegrateData functions. The integrated assay was scaled while regressing out total RNA counts and mitochondrial percentage, followed by principal component analysis. UMAP visualization and shared nearest-neighbor graph construction were performed using the

first eight principal components. Clustering resolution was evaluated across multiple values, and a final resolution of 0.09 was selected, yielding three major clusters.

Cluster marker genes were identified using Seurat FindAllMarkers with positive markers only, a minimum expression fraction of 0.25, and a log2 fold-change threshold of 0.25. Cell-cycle phase assignment was performed using Seurat CellCycleScoring with the built-in S- and G2/M-phase gene sets. The proportions of G1, S, and G2/M phase cells were calculated for each treatment group and cluster. Expression of selected genes was visualized using Seurat FeaturePlot, Dotplot and VlnPlot functions.

For pathway analysis, differential expression between pacritinib-treated and control cells was performed within each cluster using Seurat FindMarkers with pacritinib as ident.1, control as ident.2, min.pct = 0.25, and logfc.threshold = 0. Genes were ranked by average log2 fold change, and gene set enrichment analysis was performed using fgsea against MSigDB KEGG gene sets with minSize = 15, maxSize = 500, and 1,000 permutations.

Establishment and culture of human HCC organoids

Single cells were resuspended in growth factor-reduced Matrigel (Corning, NY, USA) at a density of 1,000–2,000 cells per 20 µL and seeded into pre-warmed 48-well plates. After polymerization at 37°C for 40 min, 300 µL of organoid culture medium was added to each well. The organoid culture medium consisted of Advanced DMEM/F12 supplemented with 1× GlutaMAX, 10 mM HEPES, 1× B27, 1× N2, 1.25 mM N-acetylcysteine, 10 mM nicotinamide, 10 nM gastrin I, 500 nM A83-01, 3 nM dexamethasone, 10 µM forskolin, 1× penicillin-streptomycin, 50 ng/mL Primocin, 50 ng/mL epidermal growth factor (EGF), 100 ng/mL fibroblast growth factor 10 (FGF10), 25 ng/mL hepatocyte growth factor (HGF), and 10 µM Y-27632. Y-27632 was included only during the initial 4 days of culture and was omitted thereafter. The culture medium was replaced every 2 days. For routine passaging, organoids were recovered from Matrigel using Cell Recovery Solution, dissociated into single cells with Trypsin-EDTA, re-embedded in fresh Matrigel, and cultured under the same conditions.

Organoid growth analysis and live-cell-imaging of cell death

HCC organoids were seeded into 96-well plates and allowed to establish before treatment with the indicated compounds (pacritinib or sorafenib). Organoid growth was quantified using the CellTiter-Glo® 3D Cell Viability Assay (Promega, WI, USA) according to the manufacturer's instructions. Luminescence was measured using an EnSpire Alpha multimode plate reader (PerkinElmer, MA, USA).

For live-cell imaging, organoids were stained with DiYO-3 (AAT Bioquest, #17581) according to the manufacturer's instructions. Time-lapse fluorescence images were acquired using an Etaluma LS850 live-cell imaging microscope (Etaluma, CA, USA).

Xenograft study

All animal experiments were conducted in accordance with

the guidelines of Korean Food and Drug Administration. Protocols were reviewed

and approved by the Institutional Animal Care and Use Committee of the Korea Research Institute of Chemical Technology (KRICT). Six-week-old male BALB/c nude mice (BALB/c nu/nu; JaBio Inc., Suwon, Korea) were acclimated for 1 week before experiments. At 7 weeks of age, mice were subcutaneously injected in the dorsal flank with 2×10^6 HCC organoid #6 cells suspended in 200 µL of DPBS and Matrigel (1:1, v/v; Corning). When tumors reached approximately 50 mm^3, mice were randomly assigned to vehicle or pacritinib treatment groups (n = 5 per group). Pacritinib (MedChemExpress, NJ, USA) was suspended in a vehicle containing 1% methylcellulose (50%, v/v), Tween-80 (1%, v/v), and distilled water (49%, v/v) and administered by oral gavage once daily at 150 mg/kg for 9 consecutive days. Tumor dimensions and body weight were measured daily. All animal experiments were approved by the Institutional Animal Care and Use Committee of the Korea Research Institute of Chemical Technology (KRICT) (Approval No. 2024-6C-11-01) and were conducted in accordance with the institutional guidelines.

Human tissue samples and tissue microarray

Formalin-fixed, paraffin-embedded (FFPE) human liver disease spectrum tissue microarray slides (LV20812b) were purchased from TissueArray.Com (MD, USA). The tissue microarray contained normal liver, hepatitis, hepatic cirrhosis, and HCC tissues with corresponding clinicopathological information provided by the manufacturer. Tissue sections were subjected to immunohistochemical staining for JAK2, phospho-JAK2 (Tyr221), FLT3, and phospho-FLT3 (Tyr591) as described below.

Immunohistochemistry (IHC)

FFPE tissue microarray slides and xenograft tumor tissues were deparaffinized in xylene and rehydrated through a graded ethanol series. Antigen retrieval was performed by autoclaving the sections in 0.01 M sodium citrate buffer (pH 6.0) for 20 min. The tissue sections were blocked with PBS-based mixture of 5% bovine serum albumin (GenDEPOT, TX, USA) for 30 min and were incubated overnight at 4°C with primary antibodies specific for JAK2 (Cell Signaling Technology, #3230), phospho-JAK2 (Tyr221; Thermo Fisher Scientific, #PA5-36854), FLT3 (Thermo Fisher Scientific, #PA5-34448), phospho-FLT3 (Tyr591; Thermo Fisher Scientific, #PA5-105884), Ki-67 (Abcam, #ab16667), and cleaved PARP1 (Abcam, #ab32064). After primary antibody incubation, sections were processed using a SPlink HRP Rabbit DAB Detection Kit (OriGene, MD, USA, #D03-18), including incubation with a biotinylated secondary antibody for 30 min followed by HRP-streptavidin for 30 min at room temperature according to the manufacturer's instructions. After washing with PBS, immunoreactivity was visualized using 3,3'-diaminobenzidine (DAB) substrate (Abcam, #ab64238) and counterstained with hematoxylin. Bright-field images of tissue microarray sections were captured using a DMi8 microscope (Leica Microsystems, Wetzlar, Germany), and DAB-stained xenograft tumor sections were imaged using a Nuance FX multispectral imaging system (PerkinElmer, MA, USA). Immunostaining was quantified using ImageJ software (National Institutes of Health, MD, USA).

Public Dataset

Gene expression data from the GSE109211_STORM dataset was obtained from the Gene Expression Omnibus (GEO) database (National Center for Biotechnology Information, MD, USA) (26). The dataset was analyzed to compare gene expression profiles between sorafenib responders and non-responders.

Statistical analysis

Statistical analyses were performed using GraphPad Prism version 11.0.2 (GraphPad Software, CA, USA). Data are presented as the mean ± standard deviation (SD). Comparisons between two groups were performed using an unpaired two-tailed Student's t-test. Statistical significance is indicated as follows: n.s. not significant, *P < 0.05, **P < 0.01, ***P < 0.001.

Results

JAK2 and FLT3 represent functionally relevant therapeutic targets in HCC

To identify clinically actionable therapeutic targets for hepatocellular carcinoma (HCC), we performed a cell-based phenotypic screen using a library of 3,200 FDA-approved compounds. Compounds exhibiting significant growth-inhibitory activity against SNU398, a primary HCC cell, were selected as primary hits. We then examined the reported molecular targets of the hit compounds based on published literature and public drug databases and categorized them according to their associated signaling pathways. This analysis revealed that components of the JAK/STAT signaling pathway accounted for the largest proportion of the identified targets (12.31%), followed by HDAC-, FLT3-, and PI3K-associated targets **(Fig. S1)**. Given the prominent representation of JAK/STAT- and FLT3-associated targets in the screening results, we next investigated the biological and therapeutic relevance of JAK2 and FLT3 in HCC.

To assess the clinical relevance of JAK2 and FLT3 during hepatocarcinogenesis, we examined their protein expression in a human liver disease progression tissue microarray comprising normal liver (n = 32), inflammatory liver (n = 48), cirrhotic liver (n = 56), and HCC tissues (n = 56). Immunohistochemical analysis revealed that the expression of both total JAK2 and phosphorylated JAK2 (p-JAK2) increased during HCC development, with the highest levels observed in HCC tissues (Fig. 1A). To determine the functional relevance of JAK2 in HCC cells, JAK2 was depleted using two independent shRNAs in HepG2 cells (**Fig. S2A**). JAK2 knockdown significantly suppressed cell proliferation throughout the experimental period compared with control cells (Fig. 1B). Consistently, colony formation assays showed that JAK2 knockdown markedly reduced both colony number and size (Fig. 1C).

Unlike JAK2, FLT3 exhibited a distinct expression pattern, with both total FLT3 and phosphorylated FLT3 (p-FLT3) levels significantly lower in HCC tissues than in normal, inflammatory, and cirrhotic liver tissues (Fig. 1D). Despite this reduction, depletion of FLT3 significantly suppressed HCC cell proliferation (**Fig. S2B and** Fig. 1E). Consistently, FLT3 depletion markedly reduced colony-forming ability, as reflected by

decreases in both colony number and size (Fig. 1F). These findings indicate that, despite their distinct expression patterns during hepatocarcinogenesis, both JAK2 and FLT3 contribute to HCC cell growth. Together with the phenotypic screening results, these data provide a biological rationale for evaluating concurrent targeting of JAK2 and FLT3 as a therapeutic strategy for HCC.

Concurrent inhibition of JAK2 and FLT3 by pacritinib suppresses HCC cell growth

Given the functional relevance of JAK2 and FLT3 in HCC, we next investigated whether their concurrent pharmacological inhibition could suppress HCC cell growth using pacritinib, a clinically available JAK2/FLT3 inhibitor (Fig. 2A). Immunoblot analysis showed that pacritinib treatment markedly reduced the phosphorylation of JAK2 and its downstream effector STAT3 and concurrently suppressed FLT3 phosphorylation in HepG2, Hep3B, Huh7, and PLC/PRF/5 cells in a concentration-dependent manner (Fig. 2B). In addition, AKT phosphorylation was substantially reduced following pacritinib treatment, indicating concurrent suppression of the PI3K/AKT signaling pathway (Fig. 2B). Consistent with these molecular effects, pacritinib potently inhibited cell proliferation in all four HCC cell lines in a concentration-dependent manner (Fig. 2C). Colony formation assays further demonstrated that pacritinib markedly suppressed clonogenic growth, as evidenced by dose-dependent reductions in both colony number and colony area (Fig. 2D). Collectively, these findings demonstrate that inhibition of JAK2 and FLT3 signaling by pacritinib effectively suppresses HCC cell proliferation and clonogenic capacity.

Pacritinib induces cell-cycle arrest and suppresses proliferative transcriptional programs in HCC organoid #6

Given that intra-tumoral cellular heterogeneity is a major determinant of differential drug responses and therapeutic resistance (27) (25), we established six HCC organoids (**Fig. S3 and Table S1**) and investigated the response to pacritinib at single-cell resolution. Single-cell RNA sequencing (scRNA-seq) analysis revealed that HCC organoid #6 comprised three transcriptionally distinct tumor-cell clusters, reflecting cellular heterogeneity within the tumor organoid (**Fig. S4A**). Differential expression of cluster-marker genes distinguished a predominant cluster 0 from smaller cluster 1 and cluster 2 populations, with cluster 1 showing increased expression of adhesion- and extracellular matrix-associated genes such as CDH10 and POSTN, and cluster 2 showing increased expression of stress/secretory-associated genes such as FTL, S100A11, and AGR2 (**Fig. S4B-C**). Pacritinib markedly suppressed HCC organoid #6 growth (Fig. 3A). Cluster-specific GSEA supported significant suppression of JAK2 and FLT3 signaling in all three clusters following pacritinib treatment (Fig. 3B). UMAP visualization showed a broadly similar distribution of the three clusters between control and pacritinib-treated HCC organoid #6 cells, and cluster proportion analysis indicated that their relative abundance was not substantially altered by pacritinib treatment (Fig. 3C). Cluster 0 remained the predominant population, accounting for 81% and 82% of cells in the control and pacritinib-treated groups, respectively, whereas clusters 1 and 2 accounted for 13% vs. 14% and 6% vs. 4% of the total cell population, respectively. Thus, pacritinib treatment did not substantially alter the relative cellular composition of HCC organoid #6. Pathway

enrichment analysis demonstrated that all three clusters exhibited broadly comparable transcriptional responses to pacritinib, characterized by coordinated suppression of proliferation-associated gene programs, particularly those involved in ribosome biogenesis, cell cycle progression, and DNA replication (Fig. 3D). Given the prominent suppression of cell cycle-related pathways, we next examined the effects of pacritinib on cell cycle progression at single-cell resolution. Pacritinib induced a pronounced accumulation of cells in the G1 phase, accompanied by reductions in the proportions of cells in the S and G2/M phases across the three clusters (Fig. 3E). Consistent with these changes, GSEA showed strong negative enrichment of cell cycle- and DNA replication-related gene sets in all three clusters (NES = − 2.30 to − 2.69, adjusted P = 0.02–0.04) (Fig. 3F). Furthermore, pacritinib consistently reduced the expression of G1/S cell cycle regulators, including MYC, CCND1, E2F1, CDK2, and PCNA, across all three clusters (**Fig. S5A-C**). Collectively, these single-cell analyses demonstrate that pacritinib broadly suppresses proliferative transcriptional programs across transcriptionally distinct tumor-cell clusters within the representative HCC organoid model.

The anticancer effects of pacritinib in HCC organoid models

We next characterized the antitumor effects of pacritinib in HCC organoid models. Consistent with the findings obtained in HCC cell lines, pacritinib effectively inhibited the activation of JAK2 and FLT3 signaling in three independent HCC organoid models (HCC organoid #6, #7, and #8), accompanied by a marked reduction in AKT phosphorylation (Fig. 4A). Pacritinib treatment resulted in a pronounced, concentration-dependent inhibition of growth in HCC organoids. Bright-field images and quantitative viability analysis confirmed potent growth inhibition, with IC_{50} values of 0.18 μM, 0.21 μM, and 0.26 μM in HCC organoid #6, HCC organoid #7, and HCC organoid #8, respectively (Fig. 4B). Time-lapse live-cell imaging using DIVO-3 revealed that pacritinib treatment induces apoptosis of HCC organoids in a time-dependent manner, as evidenced by the progressive accumulation of DiYO-3-positive cells during pacritinib treatment (Fig. 4C). Consistently, flow cytometry analysis demonstrated a significant increase in apoptotic organoids following pacritinib exposure in all three HCC organoids (Fig. 4D). Immunoblot analysis also showed dose-dependent increase of apoptotic signaling, characterized by increased cleavage of caspase-3 and PARP in the presence of pacritinib (Fig. 4E). We therefore investigated whether pacritinib could modulate transcriptional programs associated with unfavorable prognosis in HCC (28). Heatmap analysis of genes comprising the poor-prognosis signature shows that pacritinib markedly reduced the expression of multiple signature genes (Fig. 4F). These results indicate that pacritinib attenuates a poor-prognosis-associated transcriptional program, supporting its therapeutic potential in HCC.

Pacritinib potently suppresses HCC tumor growth in vivo through inhibition of JAK2/FLT3 signaling and induction of apoptosis

To evaluate the therapeutic efficacy of pacritinib in vivo, mice bearing HCC organoid #6-derived xenografts were treated with pacritinib or vehicle. Pacritinib treatment significantly inhibited tumor

growth compared with the vehicle-treated group (Fig. 5A-B) with reduction of tumor weight (Fig. 5C), while pacritinib treatment did not cause a significant loss of body weight (**Fig. S6**). Immunoblotting analysis showed that tumors treated with pacritinib effectively suppressed the phosphorylation of JAK2, FLT3, STAT3, and AKT compared with tumors treated with vehicle. However, the total protein levels of each proteins are not altered (Fig. 5D). Consistent with in vitro results, immunohistochemical analysis of tumors treated with vehicle or pacritinib demonstrated that pacritinib effectively induces the apoptosis and suppresses the proliferation of HCC organoid #6-derived xenograft tumors (Fig. 5E). Collectively, these findings demonstrate that pacritinib effectively suppresses HCC tumor growth in vivo by simultaneously inhibiting the JAK2/FLT3 signaling axis, blocking tumor cell proliferation, and promoting apoptotic cell death.

Pacritinib exhibits superior antitumor efficacy to sorafenib in HCC

To investigate the molecular basis underlying the limited response to sorafenib in HCC, we analyzed the association between the expression of known sorafenib targets and sorafenib sensitivity using the GSE109211 dataset (26). Consistent with previous reports (16), low FLT3 expression was associated with reduced responsiveness to sorafenib in patients with HCC. Notably, JAK2 expression was increased in sorafenib non-responders, whereas other known sorafenib targets showed either no significant change or decreased expression (**Fig. S7A**). These findings prompted us to investigate whether targeting JAK2 could improve sorafenib responsiveness in the context of low FLT3 expression. We therefore depleted JAK2 using shRNA in FLT3-low PLC/PRF/5 cells (**Fig. S7B-C**). JAK2 knockdown markedly enhanced the growth-inhibitory effect of sorafenib compared with control cells (**Fig. S7D**). Based on these findings and the limited clinical benefit of sorafenib in HCC, we next asked whether simultaneous targeting of JAK2 and FLT3 with pacritinib could provide superior antitumor activity to sorafenib. Direct comparison of the two drugs in HCC cell lines showed that pacritinib exerted more potent growth-inhibitory activity than sorafenib (Fig. 6A). Consistently, colony formation assays demonstrated a greater reduction in clonogenic survival following pacritinib treatment compared with sorafenib (Fig. 6B). We further compared their antitumor activities in three independent HCC organoids. Pacritinib markedly reduced organoid growth and viability in all three HCC organoids and consistently exhibited greater antitumor activity than sorafenib (Fig. 6C-E). Overall, pacritinib showed consistently greater antitumor activity than sorafenib in both HCC cell lines and HCC organoids. We next examined whether combining pacritinib with sorafenib could enhance antitumor activity. In HCC cell lines, including HepG2, Huh7, and PLC/PRF/5, the combination showed no substantial improvement over pacritinib alone (**Fig. S8A–C**). Similar results were observed in the three HCC organoid models, where the combination increased growth inhibition relative to sorafenib alone but showed activity largely comparable to pacritinib monotherapy (**Fig. S8D–F**). Consistently, dose–response analyses showed that the activity of the combination was largely comparable to that of pacritinib monotherapy across the three HCC organoids. Taken all, these findings demonstrate that pacritinib exhibits greater antitumor activity than sorafenib, while the addition of sorafenib provides no substantial benefit over pacritinib alone.

Discussion

In this study, we show that concurrent JAK2 and FLT3 inhibition represents a potential therapeutic strategy for HCC, with pacritinib exhibiting consistent antitumor activity across multiple preclinical models and greater efficacy than sorafenib. Single-cell analysis of HCC organoid #6 revealed transcriptionally distinct tumor-cell populations, reflecting intra-tumoral heterogeneity, yet pacritinib induced comparable suppression of proliferative transcriptional programs across these populations, with no prominent intrinsically resistant population. Given the substantial molecular heterogeneity of HCC (29, 30), and variable expression of therapeutic targets (31, 32). these findings, together with the antitumor effects observed following inhibition of either JAK2 or FLT3, support concurrent targeting of both kinases as a strategy to maintain therapeutic activity across heterogeneous HCC populations. Although limited to a single organoid model, the single-cell findings provide initial evidence that this therapeutic response may be preserved across transcriptionally distinct tumor-cell populations. Collectively, these findings provide a rationale for concurrently targeting JAK2 and FLT3 as a therapeutic strategy for treating molecularly heterogeneous HCC.

The limited clinical benefit of sorafenib, particularly in patients with FLT3-low HCC, highlights the need for therapeutic strategies that can overcome limited responsiveness to sorafenib (13, 16, 33). Consistent with previous observations, our analyses further supported an association between low FLT3 expression and reduced sorafenib responsiveness in HCC. Notably, the increased JAK2 expression observed in sorafenib-resistant HCC, together with the enhanced sorafenib sensitivity following JAK2 depletion in FLT3-low HCC cells, suggests that JAK2 signaling may contribute to reduced sorafenib responsiveness when FLT3 expression is limited. These observations provide a biological rationale for targeting JAK2 alongside FLT3 in this molecular context. In contrast to the variable responses to sorafenib observed across HCC models, pacritinib exhibited consistently potent antitumor activity across models with variable JAK2 and FLT3 expression. These findings suggest that pacritinib may provide a therapeutic option for heterogeneous HCC with limited responsiveness to sorafenib.

The therapeutic relevance of pacritinib may extend beyond its direct antitumor activity. Previous studies have shown that JAK2 signaling contributes to hepatic stellate cell activation and fibrosis, and that pacritinib suppresses activated hepatic stellate cell functions and attenuates liver fibrosis and injury in experimental models of chronic liver disease (34, 35). Given that fibrosis and cirrhosis provide a major pathological background for HCC development (36, 37), these antifibrotic properties may be particularly relevant to the therapeutic application of pacritinib in HCC (34). Together with the direct antitumor activity demonstrated in the present study, these findings raise the possibility that pacritinib may have therapeutic relevance across the continuum from chronic fibrotic liver disease to established HCC. Although its potential to influence HCC development remains to be determined, the combined antifibrotic and antitumor properties of pacritinib provide additional rationale for its further investigation in HCC.

In conclusion, our findings support concurrent targeting of JAK2 and FLT3 as a therapeutic strategy for HCC and identify pacritinib as a clinically approved agent with potent antitumor activity across

molecularly heterogeneous HCC models, including FLT3-low tumors with limited sorafenib responsiveness, supporting its potential as an alternative therapeutic option to sorafenib in HCC.

Declarations

Acknowledgments

We thank Dr. Chi Hoon Park and his laboratory at the Korea Research Institute of Chemical Technology (KRICT) for kindly providing the psPAX2 and pMD2.G plasmids. We also thank einocle for performing single-cell RNA sequencing and Ngenes for conducting the analysis of clinical cancer samples.

Conflict of Interest Statement

The authors have no conflicts to report.

Author Contribution Statement

Yong-Hee Cho and Jisoo kim conceived and designed the study. Jisoo Kim, hyeran Shin, and Yonghyo Kim performed experiments. Jisoo Kim analyzed the clinical data set. Hyun-Woo Jeong performed single cell RNA sequencing data analysis. Yong-Hee Cho, Jisoo Kim and Hyun-Woo Jeong drafted the manuscript. All authors read and approved the final manuscript.

Funding Statement

This study was supported by a grant from the National Research Foundation of Korea (NRF), which was funded by the Ministry of Science (grants: RS-2023-00235550). This work was supported by the grant (KK2632-10, DK2683-01) from the Korea Research Institute of Chemical Technology

Data Availability Statement

All data are available in the manuscript or the supplementary materials. The single cell RNA sequencing datasets of HCC organoid #6 will be deposited in the NCBI Gene Expression Omnibus (GEO).

References

1. Bray F, Laversanne M, Sung H, Ferlay J, Siegel RL, Soerjomataram I, et al. Global cancer statistics 2022: GLOBOCAN estimates of incidence and mortality worldwide for 36 cancers in 185 countries. CA Cancer J Clin. 2024;74(3):229–63.
2. Vogel A, Meyer T, Sapisochin G, Salem R, Saborowski A. Hepatocellular carcinoma. Lancet. 2022;400(10360):1345–62.
3. Llovet JM, Kelley RK, Villanueva A, Singal AG, Pikarsky E, Roayaie S, et al. Hepatocellular carcinoma. Nat Reviews Disease Primers. 2021;7(1):6.

4. Finn RS, Qin S, Ikeda M, Galle PR, Ducreux M, Kim TY, et al. Atezolizumab plus Bevacizumab in Unresectable Hepatocellular Carcinoma. N Engl J Med. 2020;382(20):1894–905.
5. Cappuyns S, Corbett V, Yarchoan M, Finn RS, Llovet JM. Critical Appraisal of Guideline Recommendations on Systemic Therapies for Advanced Hepatocellular Carcinoma: A Review. JAMA Oncol. 2024;10(3):395–404.
6. Cheng AL, Qin S, Ikeda M, Galle PR, Ducreux M, Kim TY, et al. Updated efficacy and safety data from IMbrave150: Atezolizumab plus bevacizumab vs. sorafenib for unresectable hepatocellular carcinoma. J Hepatol. 2022;76(4):862–73.
7. Gordan JD, Kennedy EB, Abou-Alfa GK, Beal E, Finn RS, Gade TP, et al. Systemic Therapy for Advanced Hepatocellular Carcinoma: ASCO Guideline Update. J Clin Oncol. 2024;42(15):1830–50.
8. Villanueva A. Hepatocellular Carcinoma. N Engl J Med. 2019;380(15):1450–62.
9. Yang C, Zhang H, Zhang L, Zhu AX, Bernards R, Qin W, et al. Evolving therapeutic landscape of advanced hepatocellular carcinoma. Nat Rev Gastroenterol Hepatol. 2023;20(4):203–22.
10. Wilhelm SM, Carter C, Tang L, Wilkie D, McNabola A, Rong H, et al. BAY 43-9006 exhibits broad spectrum oral antitumor activity and targets the RAF/MEK/ERK pathway and receptor tyrosine kinases involved in tumor progression and angiogenesis. Cancer Res. 2004;64(19):7099–109.
11. Wilhelm S, Carter C, Lynch M, Lowinger T, Dumas J, Smith RA, et al. Discovery and development of sorafenib: a multikinase inhibitor for treating cancer. Nat Rev Drug Discovery. 2006;5(10):835–44.
12. Kudo M, Finn RS, Qin S, Han KH, Ikeda K, Piscaglia F, et al. Lenvatinib versus sorafenib in first-line treatment of patients with unresectable hepatocellular carcinoma: a randomised phase 3 non-inferiority trial. Lancet. 2018;391(10126):1163–73.
13. Llovet JM, Ricci S, Mazzaferro V, Hilgard P, Gane E, Blanc JF, et al. Sorafenib in advanced hepatocellular carcinoma. N Engl J Med. 2008;359(4):378–90.
14. Zhong L, Li Y, Xiong L, Wang W, Wu M, Yuan T, et al. Small molecules in targeted cancer therapy: advances, challenges, and future perspectives. Signal Transduct Target Therapy. 2021;6(1):201.
15. Stirewalt DL, Radich JP. The role of FLT3 in haematopoietic malignancies. Nat Rev Cancer. 2003;3(9):650–65.
16. Sun W, Li SC, Xu L, Zhong W, Wang ZG, Pan CZ, et al. High FLT3 Levels May Predict Sorafenib Benefit in Hepatocellular Carcinoma. Clin Cancer Res. 2020;26(16):4302–12.
17. Hin Tang JJ, Hao Thng DK, Lim JJ, Toh TB. JAK/STAT signaling in hepatocellular carcinoma. Hepatic Oncol. 2020;7(1):HEP18.
18. Mengie Ayele T, Tilahun Muche Z, Behaile Teklemariam A, Bogale Kassie A, Chekol Abebe E. Role of JAK2/STAT3 Signaling Pathway in the Tumorigenesis, Chemotherapy Resistance, and Treatment of Solid Tumors: A Systemic Review. J Inflamm Res. 2022;15:1349–64.
19. Toh TB, Lim JJ, Hooi L, Rashid M, Chow EK. Targeting Jak/Stat pathway as a therapeutic strategy against SP/CD44 + tumorigenic cells in Akt/beta-catenin-driven hepatocellular carcinoma. J Hepatol. 2020;72(1):104–18.

20. Zheng J, Wang S, Xia L, Sun Z, Chan KM, Bernards R, et al. Hepatocellular carcinoma: signaling pathways and therapeutic advances. Signal Transduct Target Therapy. 2025;10(1):35.
21. Tang W, Chen Z, Zhang W, Cheng Y, Zhang B, Wu F, et al. The mechanisms of sorafenib resistance in hepatocellular carcinoma: theoretical basis and therapeutic aspects. Signal Transduct Target Therapy. 2020;5(1):87.
22. Hart S, Goh KC, Novotny-Diermayr V, Tan YC, Madan B, Amalini C, et al. Pacritinib (SB1518), a JAK2/FLT3 inhibitor for the treatment of acute myeloid leukemia. Blood Cancer J. 2011;1(11):e44–e.
23. Mesa RA, Vannucchi AM, Mead A, Egyed M, Szoke A, Suvorov A, et al. Pacritinib versus best available therapy for the treatment of myelofibrosis irrespective of baseline cytopenias (PERSIST-1): an international, randomised, phase 3 trial. Lancet Haematol. 2017;4(5):e225–36.
24. Broutier L, Mastrogiovanni G, Verstegen MMA, Francies HE, Gavarró LM, Bradshaw CR, et al. Human primary liver cancer–derived organoid cultures for disease modeling and drug screening. Nat Med. 2017;23(12):1424–35.
25. Cho Y-H, Ro EJ, Yoon J-S, Mizutani T, Kang D-W, Park J-C, et al. 5-FU promotes stemness of colorectal cancer via p53-mediated WNT/β-catenin pathway activation. Nat Commun. 2020;11(1):5321.
26. Pinyol R, Montal R, Bassaganyas L, Sia D, Takayama T, Chau GY, et al. Molecular predictors of prevention of recurrence in HCC with sorafenib as adjuvant treatment and prognostic factors in the phase 3 STORM trial. Gut. 2019;68(6):1065–75.
27. Marusyk A, Janiszewska M, Polyak K. Intratumor Heterogeneity: The Rosetta Stone of Therapy Resistance. Cancer Cell. 2020;37(4):471–84.
28. Crouchet E, Bandiera S, Fujiwara N, Li S, El Saghire H, Fernández-Vaquero M, et al. A human liver cell-based system modeling a clinical prognostic liver signature for therapeutic discovery. Nat Commun. 2021;12(1):5525.
29. Craig AJ, von Felden J, Garcia-Lezana T, Sarcognato S, Villanueva A. Tumour evolution in hepatocellular carcinoma. Nat Reviews Gastroenterol Hepatol. 2020;17(3):139–52.
30. Zhang Q, Lou Y, Yang J, Wang J, Feng J, Zhao Y, et al. Integrated multiomic analysis reveals comprehensive tumour heterogeneity and novel immunophenotypic classification in hepatocellular carcinomas. Gut. 2019;68(11):2019–31.
31. Llovet JM, Montal R, Sia D, Finn RS. Molecular therapies and precision medicine for hepatocellular carcinoma. Nat Reviews Clin Oncol. 2018;15(10):599–616.
32. Losic B, Craig AJ, Villacorta-Martin C, Martins-Filho SN, Akers N, Chen X, et al. Intratumoral heterogeneity and clonal evolution in liver cancer. Nat Commun. 2020;11(1):291.
33. Cheng AL, Kang YK, Chen Z, Tsao CJ, Qin S, Kim JS, et al. Efficacy and safety of sorafenib in patients in the Asia-Pacific region with advanced hepatocellular carcinoma: a phase III randomised, double-blind, placebo-controlled trial. Lancet Oncol. 2009;10(1):25–34.

34. Torres S, Ortiz C, Bachtler N, Gu W, Grunewald LD, Kraus N, et al. Janus kinase 2 inhibition by pacritinib as potential therapeutic target for liver fibrosis. Hepatology. 2023;77(4):1228–40.
35. Al-Fayoumi S, Hashiguchi T, Shirakata Y, Mascarenhas J, Singer JW. Pilot study of the antifibrotic effects of the multikinase inhibitor pacritinib in a mouse model of liver fibrosis. J Exp Pharmacol. 2018;10:9–17.
36. Singal AG, Llovet JM, Yarchoan M, Mehta N, Heimbach JK, Dawson LA, et al. AASLD Practice Guidance on prevention, diagnosis, and treatment of hepatocellular carcinoma. Hepatology. 2023;78(6):1922–65.
37. Singal AG, Kanwal F, Llovet JM. Global trends in hepatocellular carcinoma epidemiology: implications for screening, prevention and therapy. Nat Reviews Clin Oncol. 2023;20(12):864–84.

Figures

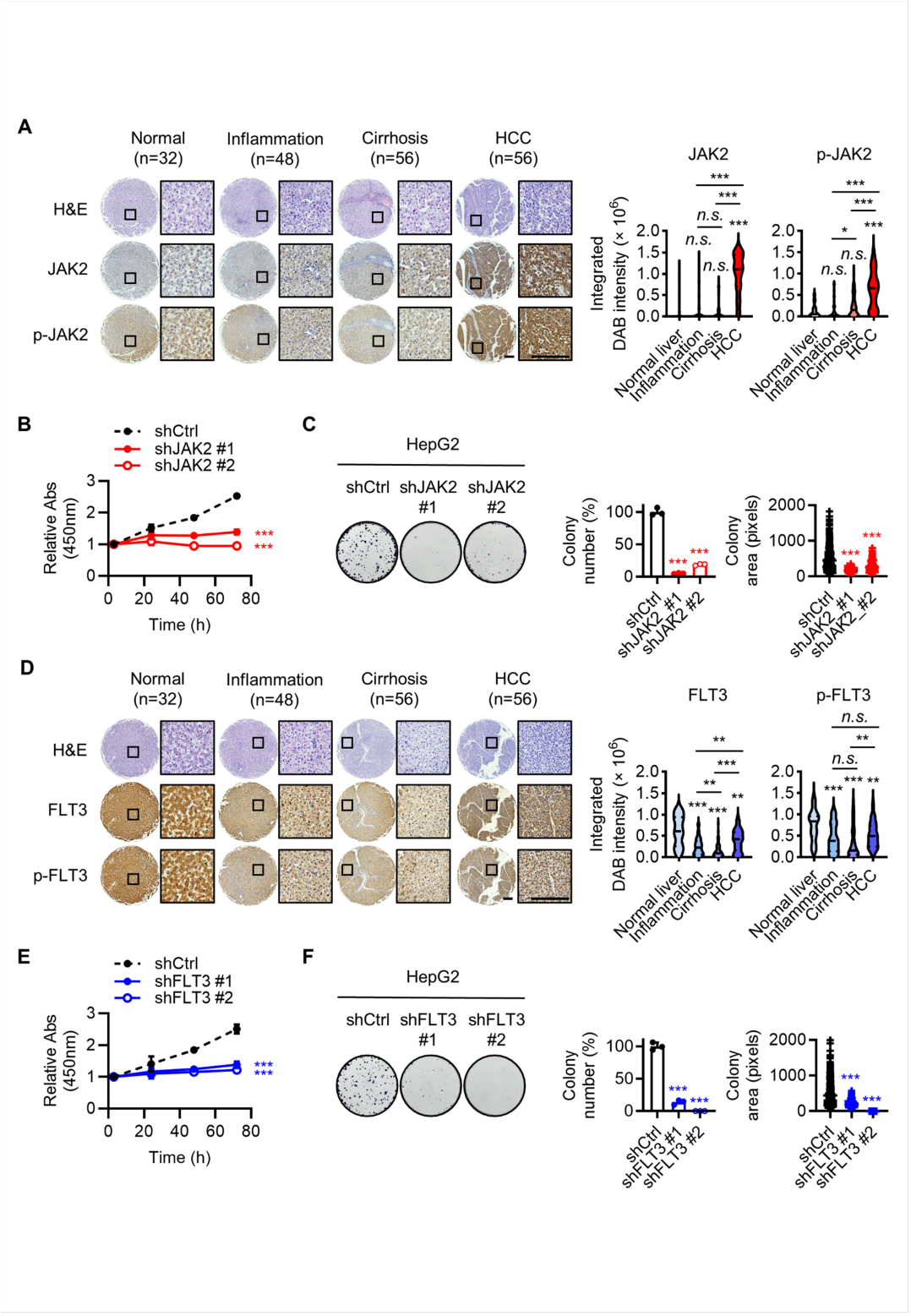


Figure 1

JAK2 and FLT3 expression in human liver disease and their therapeutic relevance in HCC.

ARepresentative hematoxylin and eosin (H&E) staining and immunohistochemical staining for JAK2 and phosphorylated JAK2 (p-JAK2) in human liver tissue microarrays comprising normal liver (n = 32), inflammation (n = 48), cirrhosis (n = 56), and hepatocellular carcinoma (HCC; n = 56). JAK2 and p-JAK2

staining was quantified as integrated DAB intensity. Scale bar, 200 μm. **B** Cell growth of HepG2 cells expressing control shRNA (shCtrl) or two independent JAK2-targeting shRNAs (shJAK2 #1 and #2), measured by relative absorbance at 450 nm at the indicated time points (n = 10). **C** Representative images and quantification of colony formation in HepG2 cells expressing shCtrl or shJAK2 #1 and #2. Colony number and colony area were quantified (n = 3). **D** Representative H&E staining and immunohistochemical staining for FLT3 and phosphorylated FLT3 (p-FLT3) in normal liver, inflammation, cirrhosis, and HCC tissues. FLT3 and p-FLT3 staining was quantified as integrated DAB intensity. Scale bar, 200 μm. **E** Cell growth of HepG2 cells expressing shCtrl or two independent FLT3-targeting shRNAs (shFLT3 #1 and #2), measured by relative absorbance at 450 nm at the indicated time points (n = 10). **F** Representative images and quantification of colony formation in HepG2 cells expressing shCtrl or shFLT3 #1 and #2. Colony number and colony area were quantified (n = 3). Data are mean ± s.d., two-sided Student's t-test, n.s., not significant, *P < 0.05, **P < 0.01, ***P < 0.001.

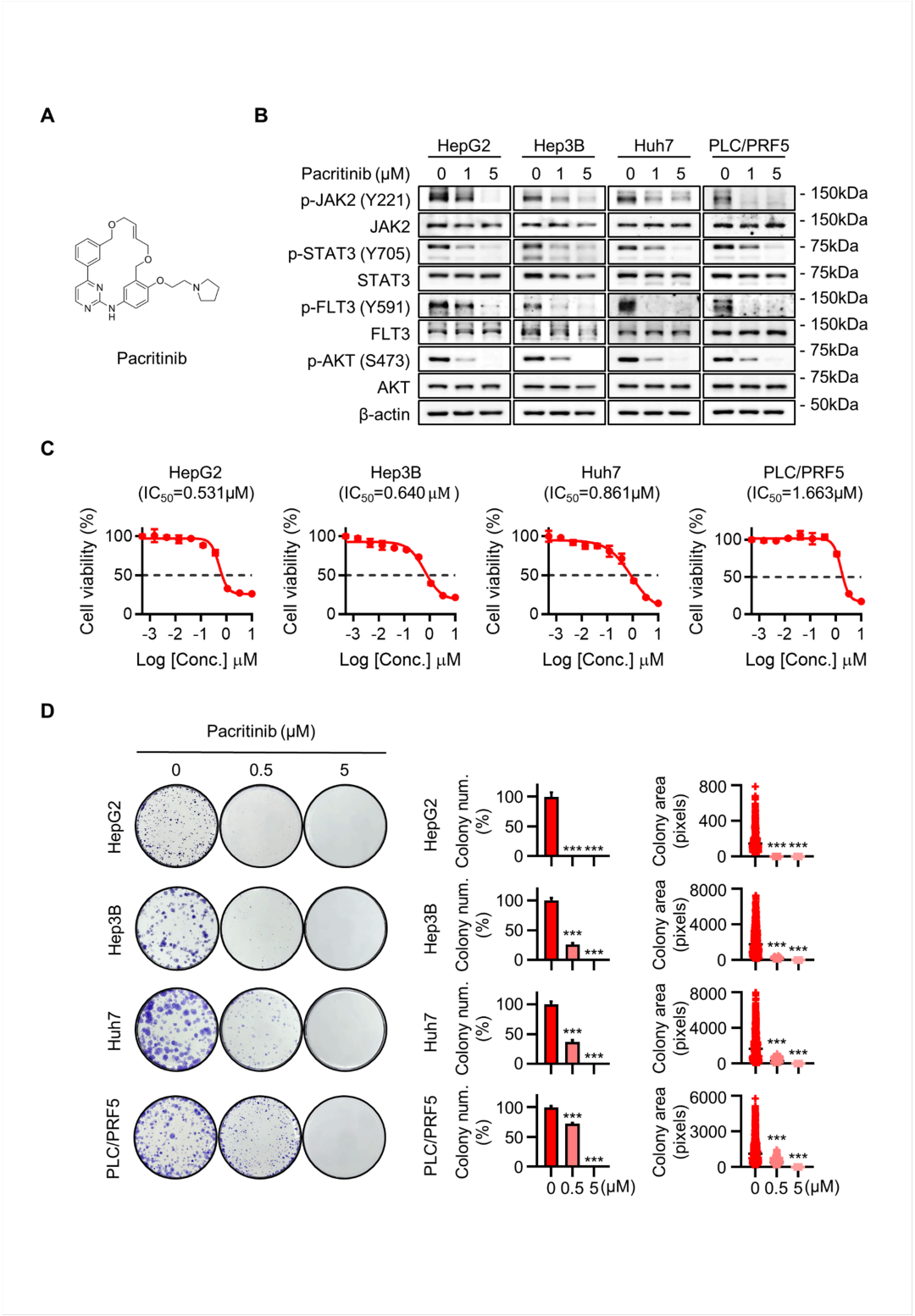


Figure 2

Anticancer effects of pacritinib in HCC cell lines.

AThe structure of pacritinib. **B**Immunoblot analysis of the phosphorylated and total forms of the indicated proteins in HepG2, Hep3B, Huh7, and PLC/PRF5 cells treated with the indicated concentrations of pacritinib for 3 h. **C**IC50 values of pacritinib for HepG2, Hep3B, Huh7, and PLC/PRF5 cells were

determined using the CytoX cell viability assay (n = 3). **D** Representative colony formation images and quantification of colony number and colony area in HepG2, Hep3B, Huh7, and PLC/PRF5 cells treated with the indicated concentrations of pacritinib (n = 3). Data are mean ± s.d., two-sided Student's t-test, n.s., not significant, *P < 0.05, **P < 0.01, ***P < 0.001.

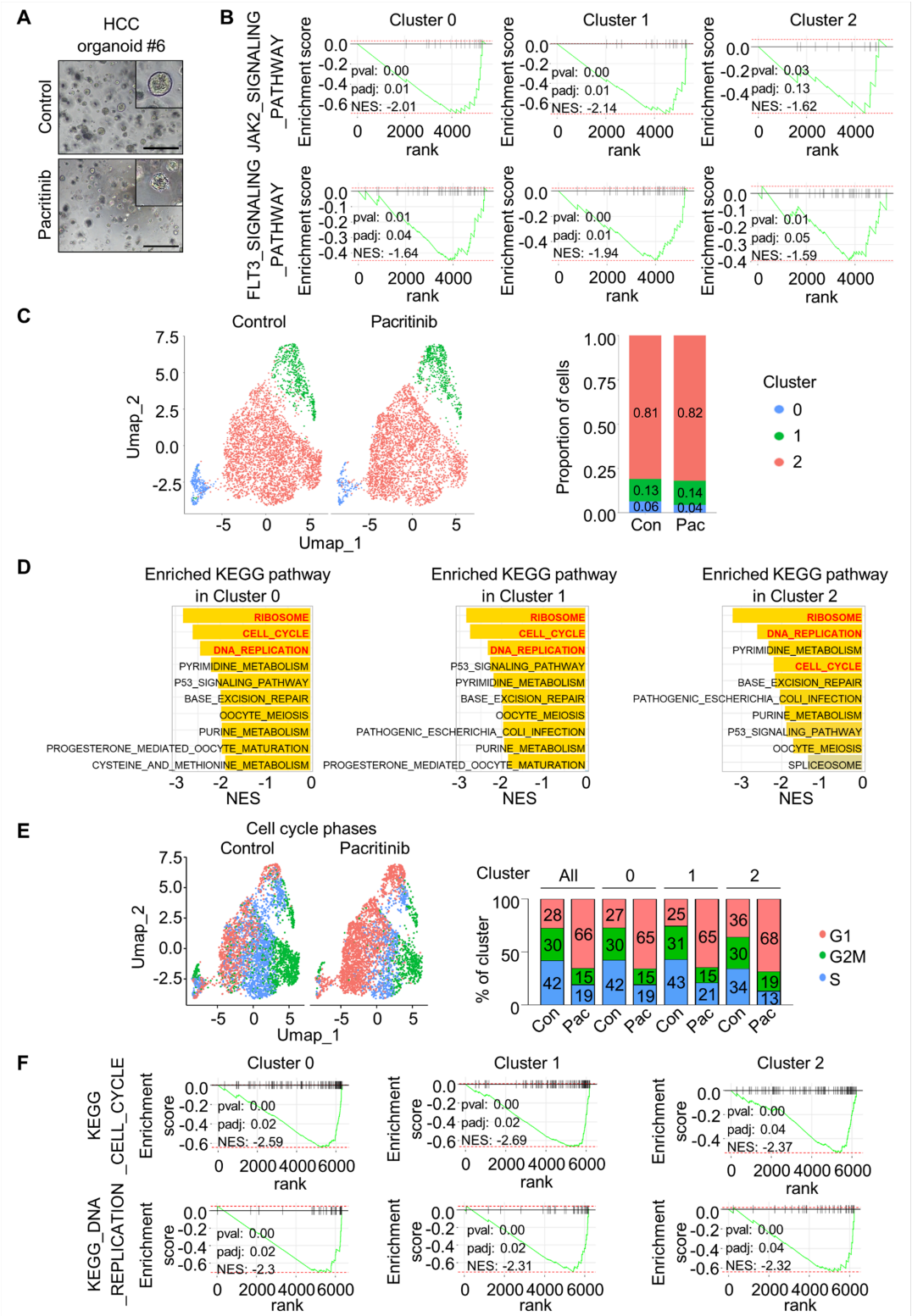


Figure 3

Therapeutic effects of pacritinib on an HCC organoid model with induction cell-cycle arrest.

ARepresentative bright-field images of HCC organoid #6 cultured for 12 days and subsequently treated with control or pacritinib (1 μM) for 2 days. Scale bar, 500 μm. **B**GSEA of the JAK2 and FLT3 signaling pathways in clusters 0, 1, and 2 of HCC organoid #6, comparing control and pacritinib-treated cells. **C** Uniform manifold approximation and projection (UMAP) plots showing the distribution of three molecularly distinct cell clusters in control (4,267 cells) and pacritinib (3,803 cells)-treated HCC organoid #6. Relative proportions of each cluster are shown. **D** Bar plots showing the top 10 downregulated KEGG pathways identified by GSEA in clusters 0, 1, and 2 following pacritinib treatment. **E**UMAP plots showing cell-cycle phase distribution and quantification of the proportions of cells in G1, S, and G2/M phase in the total population and each cluster in control and pacritinib-treated cells. **F** GSEA comparing the enrichment of KEGG cell cycle and DNA replication pathways between control and pacritinib-treated cells in clusters 0, 1, and 2.

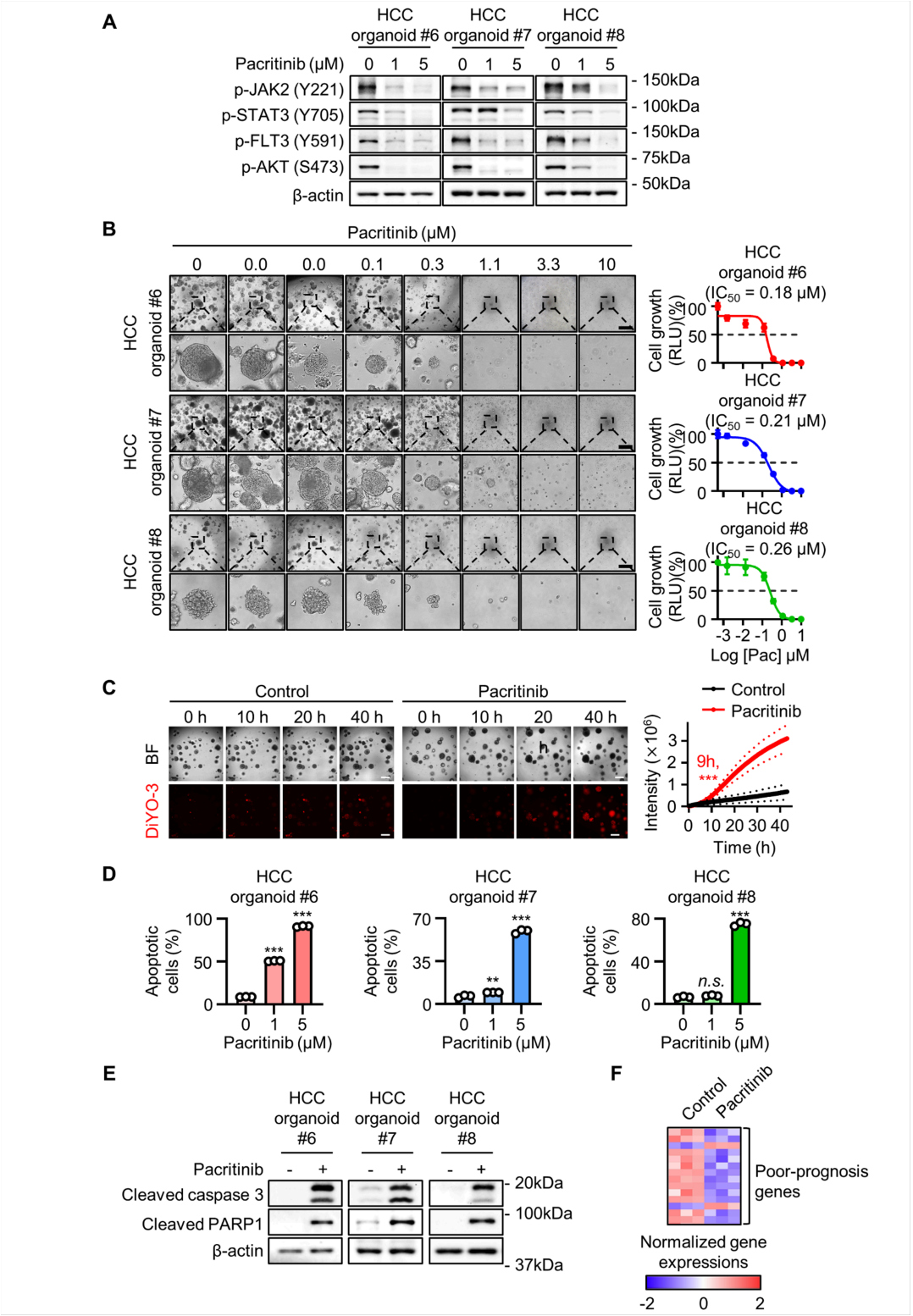


Figure 4

Effects of pacritinib on HCC organoid models with induction of apoptosis

AImmunoblot analysis of phosphorylated proteins in HCC organoids #6, #7, and #8 treated with the indicated concentrations of pacritinib for 3 h. **B** Representative bright-field images of HCC organoids #6, #7, and #8 treated with pacritinib every 2 days for 14 days (n = 3). Scale bar, 500 μm. Growth of HCC

organoids #6, #7, and #8 was assessed on day 14. **C** Representative time-lapse bright-field and DiYO-3 fluorescence images of control and pacritinib (1 μM)-treated HCC organoid #6 and quantification of DiYO-3 fluorescence intensity at the indicated time points (n = 12). Scale bar, 200 μm. **D** Quantification of apoptotic cells in HCC organoids #6, #7, and #8 treated with the indicated concentrations of pacritinib for 12 h by flow cytometry following Annexin V/PI staining (n = 3). **E** Immunoblot analysis of cleaved caspase-3 and cleaved PARP1 in HCC organoids #6, #7, and #8 treated with the indicated concentrations of pacritinib (3 μM) for 12 h. **F** Heatmap showing normalized expression levels of poor-prognosis genes in control and pacritinib-treated HCC organoid #6. Data are mean ± s.d., two-sided Student's t-test, n.s., not significant, *P < 0.05, **P < 0.01, ***P < 0.001.

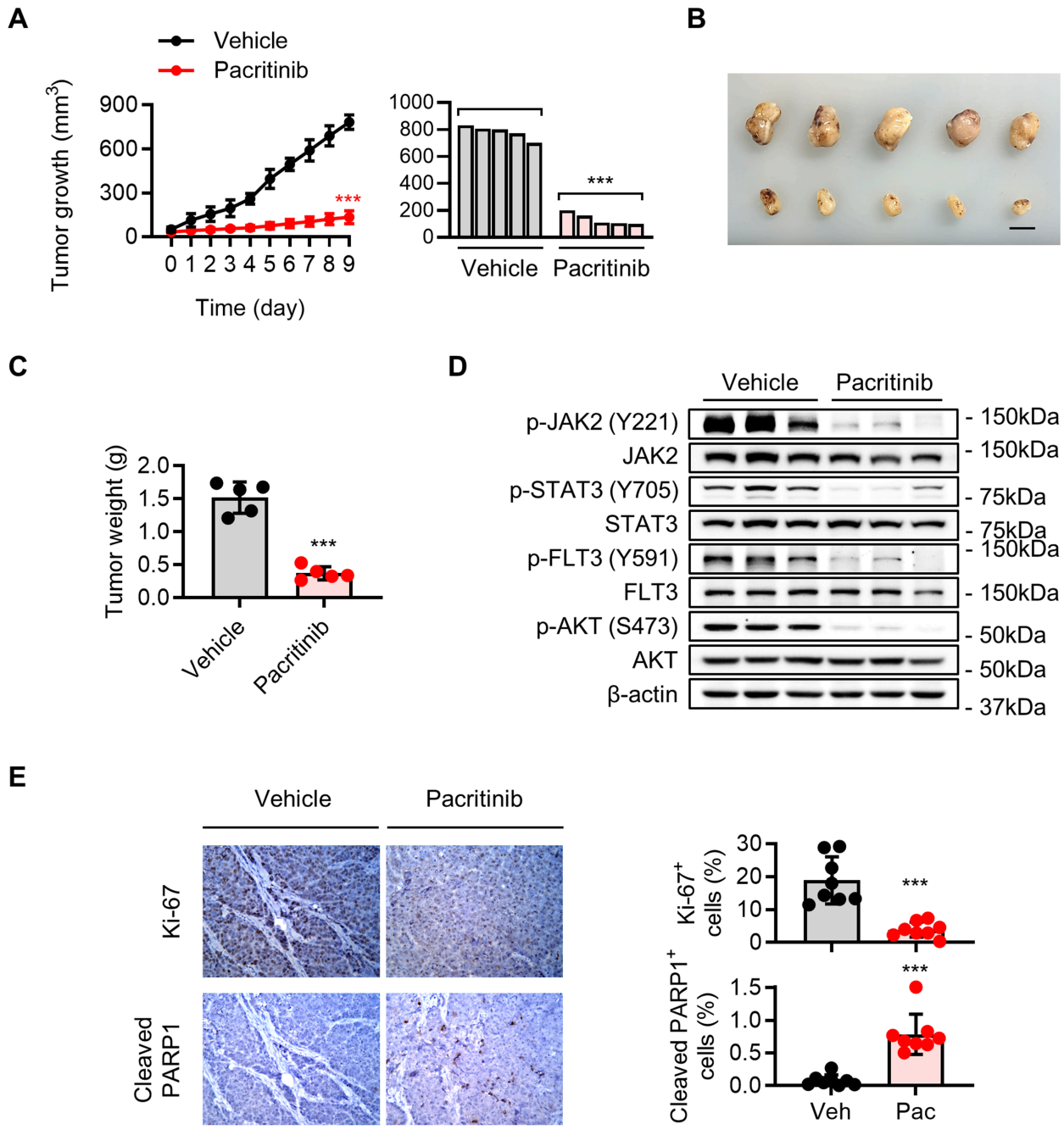


Figure 5

Anti-cancer effects of pacritinib in vivo

Mice bearing HCC organoid #6-derived xenografts were treated with vehicle or pacritinib (150 mg/kg, oral administration) daily for 9 days, and tumors were extracted and analyzed at the end of treatment. **A** Growth of tumors was measured at the indicated days after treatment and individual tumor volumes were measured at the end of treatment (n = 5 biologically independent animals per group). **B** Gross images of tumors. Scale bar, 10 mm. **C** Tumor weights measured at the end of treatment (n = 5

biologically independent animals per group). **D** Immunoblot analysis of the phosphorylated and total forms of the indicated proteins in HCC organoid #6-derived xenograft tumors treated with vehicle or pacritinib for 9 days. **E**Immunohistochemistry analysis of Ki-67 and cleaved PARP1 in sections of isolated tumors after treatment for 9 days and quantification of positive cells. (Ki-67 and cleaved PARP1, n = 8 in the vehicle and pacritinib groups). Data are mean ± s.d., two-sided Student's t-test, n.s., not significant, *P < 0.05, **P < 0.01, ***P < 0.001.

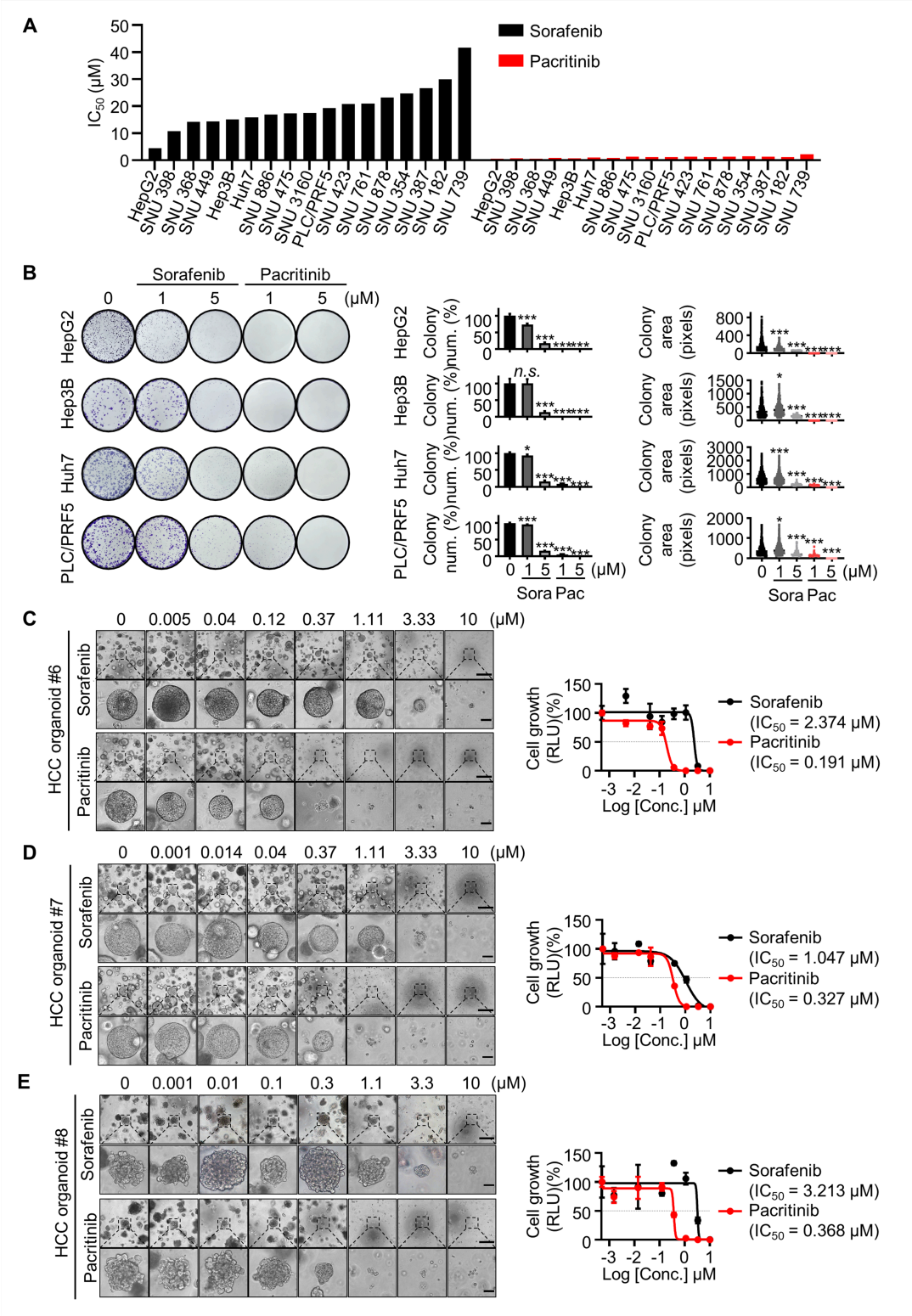


Figure 6

Superior antitumor efficacy of pacritinib than sorafenib in HCC cells and HCC organoid models.

A IC_{50} values of sorafenib and pacritinib in the indicated HCC cells. **B** Representative colony formation images and quantification of colony number and colony area in HepG2, Hep3B, Huh7, and PLC/PRF5 cells treated with the indicated concentrations of sorafenib and pacritinib (control, n = 6; each pacritinib-treated group, n = 3). **C-E** Representative bright-field images of HCC organoid #6, HCC organoid #7, and HCC organoid #8 treated with sorafenib or pacritinib every 2 days for 14 days (n = 3). Scale bar, 500 μm. Growth of HCC organoids was assessed on day 14. Data are mean ± s.d., two-sided Student's t-test, n.s., not significant, *P < 0.05, **P < 0.01, ***P < 0.001.

Supplementary Files

This is a list of supplementary files associated with this preprint. Click to download.

- CancerCellInternationalSupplementarymaterials.docx